

Article

Reaction Mechanism of ZrB₂-ZrC Formation in Ni-Zr-B₄C System Analyzed by Differential Scanning Calorimetry

Jiaying Xu ^{1,*}, Pengfei Ma ¹ and Binglin Zou ²¹ Jilin Institute of Chemical Technology, College of Science, Jilin 132022, China; mapf@jlict.edu.cn² State Key Laboratory of Rare Earth Resources Utilization, Changchun Institute of Applied Chemistry, Chinese Academy of Sciences, Changchun 130022, China; zoubinglin@ciac.ac.cn

* Correspondence: xujiaying@jlict.edu.cn; Tel.: +86-187-44220760

Abstract: The reaction mechanism of ZrB₂-ZrC formation in a 30% Ni-Zr-B₄C system under argon was revealed by using differential scanning calorimetry (DSC), X-ray diffraction (XRD) and scanning electron microscopy (SEM). The results indicated that the reaction mechanism in the Ni-Zr-B₄C system was complex. Initially, Ni_xZr_y and Ni_xB_y intermetallics were formed via solid-state diffusion reactions between Ni, B₄C and Zr. Then, the eutectic reaction between Ni₂B and Ni₄B₃ lead to the formation of Ni-B liquid. The free C atoms dissolved into the Ni-B liquid to form a Ni-B-C ternary liquid, and then part of the Zr powder dissolved into the surrounding Ni-B-C ternary liquid to form Ni-Zr-B-C quaternary liquid. Finally, ZrB₂ and ZrC formed and precipitated out of the saturated liquid. The eutectic liquid plays an important role during the formation of ZrB₂-ZrC.

Keywords: reaction mechanism; ZrB₂-ZrC; combustion synthesis; self-propagation high-temperature synthesis; differential scanning calorimetry



Citation: Xu, J.; Ma, P.; Zou, B. Reaction Mechanism of ZrB₂-ZrC Formation in Ni-Zr-B₄C System Analyzed by Differential Scanning Calorimetry. *Materials* **2021**, *14*, 6467. <https://doi.org/10.3390/ma14216467>

Academic Editor: Andrzej Dziejcz

Received: 16 September 2021

Accepted: 26 October 2021

Published: 28 October 2021

Publisher's Note: MDPI stays neutral with regard to jurisdictional claims in published maps and institutional affiliations.



Copyright: © 2021 by the authors. Licensee MDPI, Basel, Switzerland. This article is an open access article distributed under the terms and conditions of the Creative Commons Attribution (CC BY) license (<https://creativecommons.org/licenses/by/4.0/>).

1. Introduction

Boride and carbide of zirconium (ZrB₂ and ZrC) exhibit outstanding properties such as high hardness and melting points, low density as well as high resistance to corrosion and wear, which makes them attractive candidates for high-temperature ceramics, cutting tools, corrosion-resistant parts, reinforcing particles in the composites and wear resistant coatings [1–6]. It is believed that double or multiple phase ceramics have better properties than single-phase ceramics [7–9]. Hence, more attention has been paid to develop materials combining ZrB₂ and ZrC ceramics [1–5].

Multiphase ceramics can be synthesized by a variety of methods including hot isostatic pressing, spark plasma sintering, pressureless sintering, combustion synthesis, etc. [10–13]. Among them, combustion synthesis (CS) has attracted much attention for preparation of intermetallics, borides, carbides, nitrides and silicides due to the advantages of simple devices, low processing cost, high reaction purity and fast reaction rates [14–18]. CS is generally divided into two types. The first is self-propagating high-temperature synthesis (SHS) by ignition and spread at one end of the sample, and the second is thermal explosion (TE) by heating the whole sample uniformly [19,20]. Up to now, ZrB₂-ZrC/Al, ZrB₂-ZrC/Cu and ZrB₂-ZrC/Co composites have been successfully prepared by the SHS method [1–5].

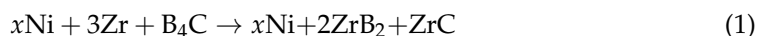
In a previous paper [21], we successfully synthesized ZrC-ZrB₂/Ni cermet powders using a Ni-Zr-B₄C system by the SHS method. The SHS-derived feedstock powders were deposited on a magnesium alloy, and atmospheric plasma spraying was used to obtain ZrC-ZrB₂/Ni cermet coatings. However, the reaction mechanism of ZrB₂-ZrC formation in the Ni-Zr-B₄C system needs to be further studied.

In the present work, differential scanning calorimetry (DSC), X-ray diffraction (XRD) and scanning electron microscopy (SEM) were used to reveal the formation mechanism of ZrB₂-ZrC in the Ni-Zr-B₄C system during combustion synthesis. It is expected that

these preliminary results will be valuable for promoting the understanding of the reaction mechanism of ZrB₂-ZrC formation in the Ni-Zr-B₄C system.

2. Materials and Methods

The ZrB₂-ZrC/Ni composites were produced according to the following reaction equation:



Commercial powders Ni (~99% in purity, ≤48 μm, ST-nano science and technology Ltd. Co., Shanghai, China), Zr (~99% in purity, ≤38 μm, ST-nano science and technology Ltd. Co., Shanghai, China) and B₄C (~95% in purity, ≤3.5 μm, Abrasive Ltd. Co., Dunhua, China) were selected as the starting materials. In order to investigate the complex combustion reactions in the Ni-Zr-B₄C system, DSC experiments were performed on the mixtures of Zr-B₄C, Ni-B₄C, Ni-Zr and 30 wt.% Ni-Zr-B₄C. In 30 wt.% Ni-Zr-B₄C mixture, Zr and B₄C powders with a molar ratio of 3:1 were mixed with 30 wt.% Ni. The compositional proportions in the Zr-B₄C, Ni-B₄C and Ni-Zr mixtures were in accordance with those in the 30 wt.% Ni-Zr-B₄C mixture. The weight of powder mixtures subjected to DSC analysis was 15 mg. The reactant mixtures were dry-mixed sufficiently in a container using zirconia balls at a low speed (~50 rpm) for 6 h.

DSC was carried out on a STA 449C Jupiter (Netzsch, Weimar, Germany) apparatus to reveal the reaction mechanism of the Ni-Zr-B₄C system. The heating process was set to a rate of 10 °C/min in flowing argon gas (99.9% in purity, flow rate: 40 mL/min). Following DSC analysis, the sintered powders were crushed, and the phase composition was analyzed by XRD (D8 Advance, Bruker, Ettlingen, Germany, Cu-Kα radiation, λ = 0.15406 nm) at a scanning speed of 6°/min and a scanning range of 20–80°. Microstructures of the reacted samples were characterized by SEM (S-4800, Hitachi, Tokyo, Japan) equipped with an energy-dispersive spectrometer (EDS).

3. Results and Discussion

Figure 1 displays the DSC curves of the Zr-B₄C, Ni-B₄C, Ni-Zr and 30 wt.% Ni-Zr-B₄C mixtures heated to 1200 °C with a heating rate of 10 °C/min. Moreover, interrupted experiments were performed in order to elucidate the reaction mechanism during the heating process.

The DSC curve of the Zr-B₄C mixture is shown in Figure 1a. A broad exothermic peak appears near 1008 °C. The XRD result of DSC product heated to 1200 °C shows that the product mainly consists of a large amount of ZrB₂, ZrC and a small amount of Zr (see Figure 2). The presence of Zr may have been caused by the incomplete reaction of reactants. Hu et al. [1] studied the mechanism of ZrB₂ and ZrC generation in the Zr-B₄C system and proposed that the solid-phase synthesis reaction was the main formation mechanism. Zhang et al. [2–4] investigated the reaction behavior and formation mechanism in the Cu-Zr-B₄C system. Effects of heating rate and B₄C particle size on the reaction process in the Zr-B₄C system were also explored. Either increasing the particle size of B₄C or increasing the heating rate may result in a sluggish solid-state reaction between Zr and B₄C, which leads to the residual of Zr and B₄C in the DSC products. The diffraction peaks of Zr were also found in the XRD patterns of the above research, but the diffraction peaks of B₄C were very weak or absent due to the atomic characteristics and crystalline lattice of B₄C [1–4].

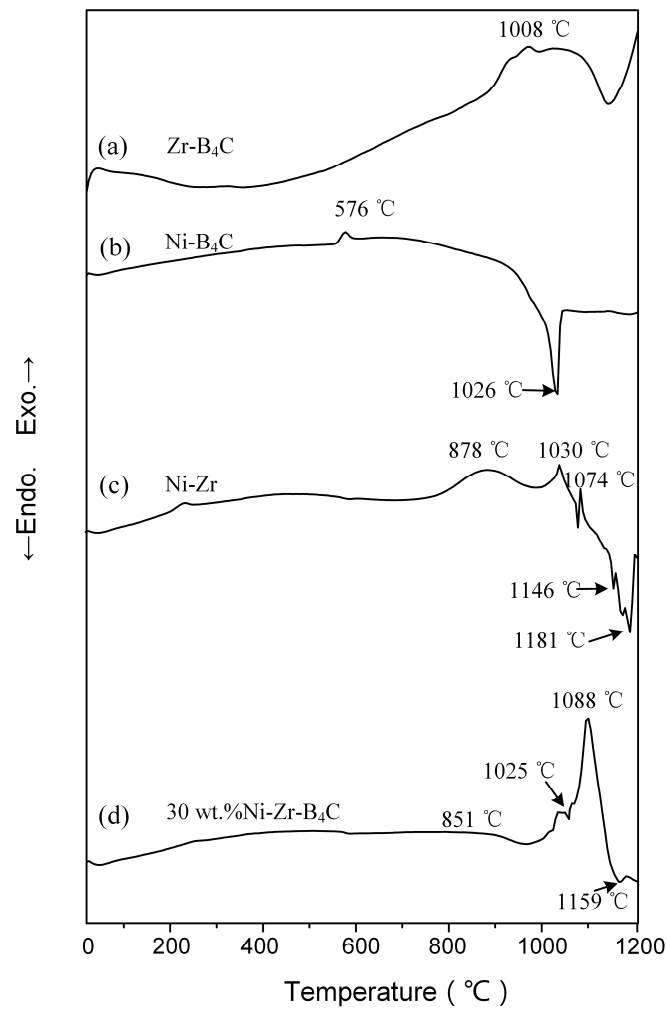


Figure 1. The DSC curves of the mixtures heated to 1200 °C with a heating rate of 10 °C/min: (a) Zr-B₄C; (b) Ni-B₄C; (c) Ni-Zr and (d) 30 wt.% Ni-Zr-B₄C.

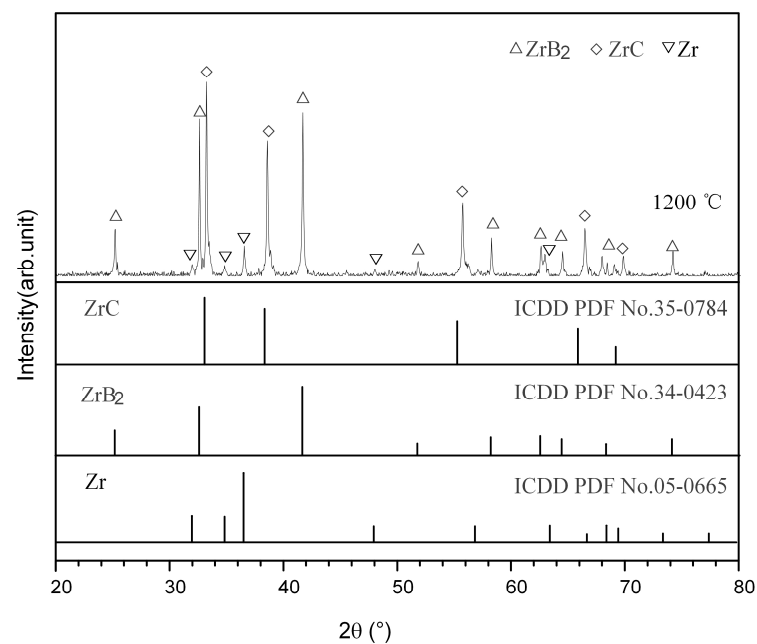


Figure 2. XRD pattern for the DSC product of the Zr-B₄C mixture heated to 1200 °C.

Figure 1b shows the DSC curve of the Ni-B₄C mixture heated to 1200 °C. A small exothermic peak was present at 576 °C, and a large endothermic peak was present at 1026 °C. To better interpret the two peaks, the Ni-B₄C mixtures were heated to 900 °C and 1030 °C, respectively, before being cooled down. Figure 3 shows the XRD patterns obtained for DSC products when quenched from 900 °C, 1030 °C and 1200 °C, respectively. When the DSC heating was quenched from 900 °C, the product was mainly composed of Ni₂B, Ni₃B and C, indicating that the solid reaction between Ni and B₄C occurred at this time, corresponding to the exothermic peak appearing at 576 °C on the DSC curve. As shown in Figure 3, the DSC product quenched from 1030 °C was mainly composed of Ni₂B, o-Ni₄B₃ and a small amount of NiC₃B₁₅. When the Ni-B₄C mixture was heated to 1200 °C, o-Ni₄B₃, m-Ni₄B₃ and a small amount of Ni₂B and NiC₃B₁₅ were formed in the product. Following the Ni-B binary phase diagram [22], a Ni-B melt could be formed due to the eutectic reaction between Ni₂B and o-Ni₄B₃ at 1018 °C, which corresponded to the large endothermic peak at 1026 °C on the DSC curve. At the same time, the Ni-B liquid phase could promote the dissolution of C atoms and form the Ni-B-C melt. The NiC₃B₁₅ phase was possibly formed and precipitated from it during the cooling process.

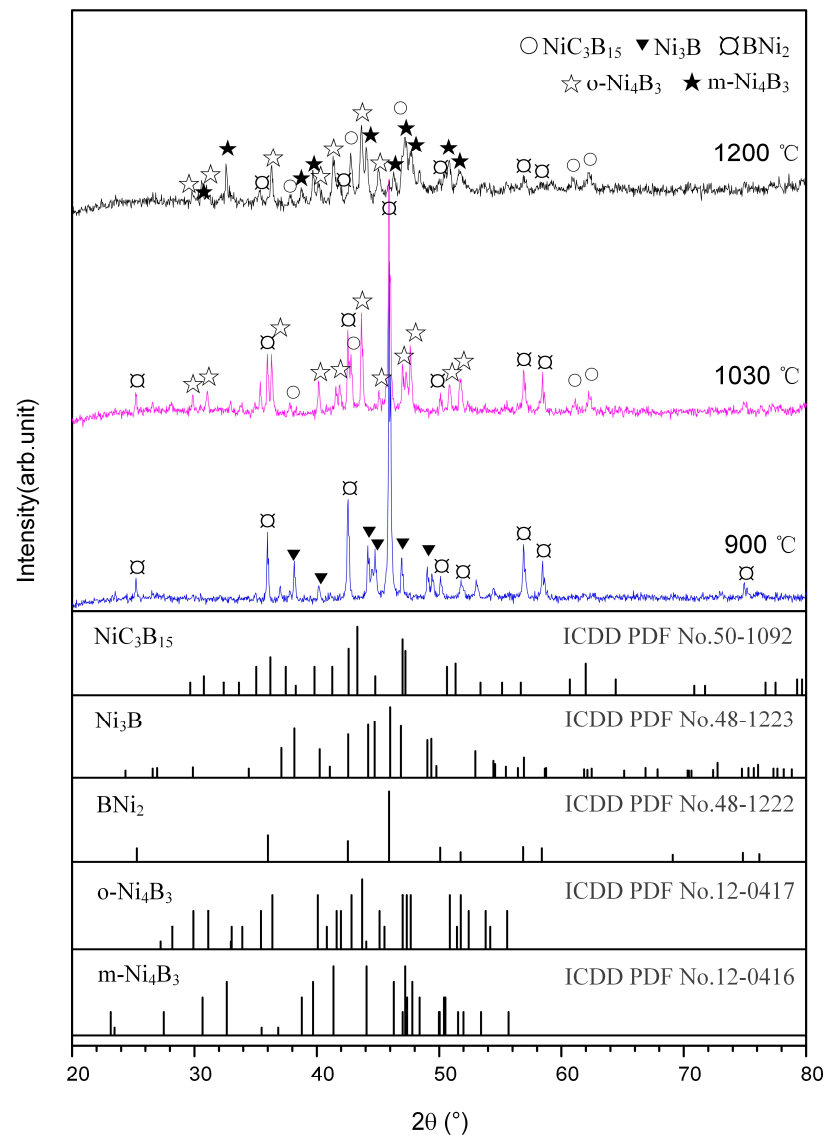


Figure 3. XRD patterns for the DSC products of Ni-B₄C mixtures quenched at different temperatures.

Figure 1c shows the DSC curve of the Ni-Zr mixture heated to 1200 °C. As indicated, three exothermic peaks appear at 878 °C, 1030 °C and 1074 °C, respectively. Two endothermic peaks appear at 1146 °C and 1181 °C. In order to determine the reactions occurring near these peaks, the Ni-Zr mixtures were heated to 600 °C, 950 °C, 1030 °C, 1080 °C, 1160 °C and 1200 °C, respectively, and then cooled down. XRD patterns for the DSC products of Ni-Zr mixtures quenched at different temperatures are shown in Figure 4. When the Ni-Zr mixture was heated to 600 °C, only the original reactants Ni and Zr were found in the quenched product, and no obvious reaction occurred (see Figure 4). When the Ni-Zr mixture was heated to 950 °C, the diffraction peak intensity of Ni and Zr in the quenched product was obviously weakened. At this time, NiZr, Ni₁₀Zr₇ and Ni₅Zr were generated, which indicated that there was a solid-state reaction between Ni and Zr, resulting in a wide exothermic peak at 878 °C. When the Ni-Zr mixture was heated to 1030 °C, the content of Ni₁₀Zr₇ increased significantly, which corresponded to the exothermic peak at 1030 °C (see Figure 4). As the temperature was raised to 1080 °C, the Ni₁₁Zr₉ phase appeared, and the content of unreacted Ni and Zr decreased significantly. The production of Ni₁₁Zr₉ led to the presence of an exothermic peak at 1074 °C. As the temperature was raised to 1160 °C, Ni₁₀Zr₇ disappeared, and there was a large amount of NiZr and a small amount of Ni₁₁Zr₉ in the product. Following the Ni-Zr binary phase diagram [23], Ni₁₀Zr₇ and Ni will form a eutectic liquid at 1150 °C, which exactly corresponds to the endothermic peak at 1146 °C in the DSC curve. When the Ni-Zr mixture was heated to 1200 °C, the product mainly consisted of NiZr, Ni₁₁Zr₉ and a small amount of NiZr₂, in which the content of Ni₁₁Zr₉ phase increased obviously. According to the Ni-Zr binary phase diagram [23], NiZr and Ni will form eutectic liquid phase at 1170 °C. Therefore, it can be deduced that the Ni-Zr eutectic liquid will form after the temperature is gradually raised to 1170 °C, which leads to the endothermic peak at 1181 °C. Subsequently, when the mixture was heated to 1200 °C and then cooled down, Ni₁₁Zr₉ and NiZr₂ eventually crystallized from the Ni-Zr eutectic liquid.

Figure 1d shows the DSC curve of the 30 wt.% Ni-Zr-B₄C mixture heated to 1200 °C. As shown, two exothermic peaks were observed at 851 °C and 1088 °C, and two endothermic peaks were observed at 1025 °C and 1159 °C, respectively. In order to make clear the reactions occurring during the heating process, DSC interrupted experiments were carried out for the Ni-Zr-B₄C mixtures at 900 °C, 1030 °C, 1060 °C, 1100 °C, 1130 °C, 1170 °C and 1200 °C, respectively, and then cooled down. The XRD patterns for the DSC products quenched at different temperatures are shown in Figure 5. When the Ni-Zr-B₄C mixture was heated to 900 °C, a large amount of Ni₂B and a small quantity of Ni₄B₃, NiZr and Ni₅Zr were generated in the product, indicating that the wide exothermic peak near 851 °C corresponded to the formation of these Ni_xZr_y and Ni_xB_y phases. This is also consistent with the previous analysis of Ni-Zr and Ni-B mixtures. When the Ni-Zr-B₄C mixture was heated to 1030 °C, a very small amount of ZrB₂ and ZrC appeared in the product, indicating that a small amount of Zr reacted with B₄C at this time. As the temperature was raised to 1060 °C, the diffraction peak intensity of Ni₂B and Ni₄B₃ decreased. According to the analysis of the Ni-B₄C mixture, Ni₂B and Ni₄B₃ can form the Ni-B eutectic liquid at 1018 °C, which corresponds to the endothermic peak at 1025 °C in the DSC curve of Ni-Zr-B₄C. At the same time, the formation of the Ni-B liquid phase also promotes the contact and reaction between the reactants in the mixture, and the free C atomic can dissolve into the Ni-B liquid phase to form the Ni-B-C ternary liquid phase, which fully contacts with the surrounding Zr powder and B₄C powder. As the temperature was raised to 1100 °C, a large amount of Ni, ZrB₂ and ZrC were formed in the product, and a large exothermic peak appeared at 1088 °C in the DSC curve. It is speculated that part of the Zr powder directly reacted with B₄C to form ZrB₂ and ZrC, and part of the Zr powder dissolved into the surrounding Ni-B-C ternary liquid to form Ni-Zr-B-C quaternary liquid. When the concentration of [Zr], [B] and [C] atoms in the Ni-Zr-B-C liquid achieved the thermodynamic condition for the formation of ZrB₂ and ZrC, ZrB₂ and ZrC particles precipitated out of the saturated liquid. It is worth mentioning that a large amount of Ni₁₀Zr₇ also appeared in the product

at 1100 °C, which was slightly different from the temperature at which Ni₁₀Zr₇ appeared in large quantities in the Ni-Zr mixture (1030 °C), which may be due to the influence of the addition of B₄C in the Ni-Zr-B₄C mixture. When the Ni-Zr-B₄C mixture was heated to 1130 °C, the product was mainly composed of a large amount of ZrB₂, ZrC and a small amount of Ni₁₀Zr₇ and Ni₂B. When the Ni-Zr-B₄C mixture was heated to 1170 °C, the product consisted of ZrB₂, ZrC, Ni and a small amount of Ni₂B. As the temperature was raised to 1200 °C, the product consisted of ZrB₂, ZrC and Ni, indicating that the reaction of the system had tended to be complete. When the temperature rose from 1130 °C to 1170 °C, the content of Ni₁₀Zr₇ decreased rapidly, which was consistent with the results in the previously studied Ni-Zr mixture. When the temperature reached 1150 °C, Ni₁₀Zr₇ and Ni could form a Ni-Zr eutectic liquid phase, corresponding to the thermal absorption peak at 1159 °C in the DSC curve of the Ni-Zr-B₄C mixture. The formation of Ni-Zr liquid phase promotes the contact and reaction between each component, which makes the reaction of the whole system fast and complete.

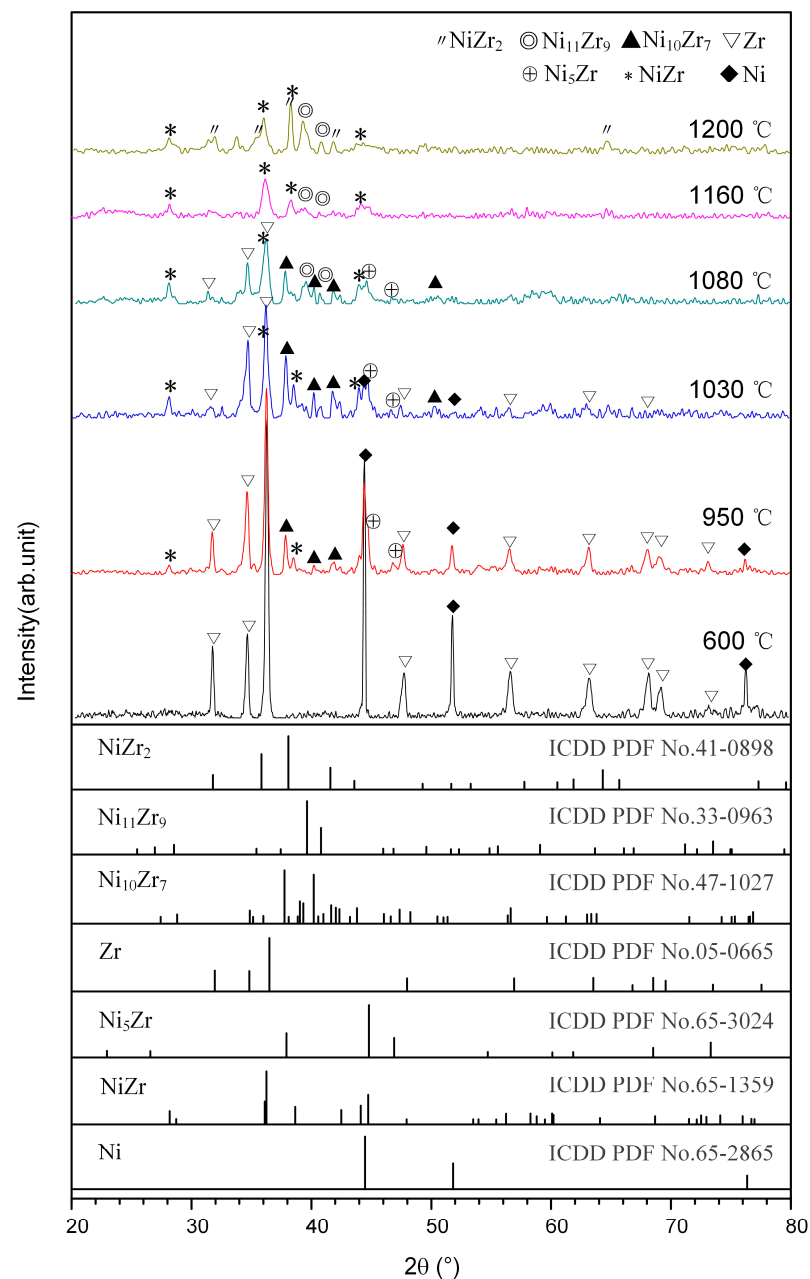


Figure 4. XRD patterns for the DSC products of Ni-Zr mixtures quenched at different temperatures.

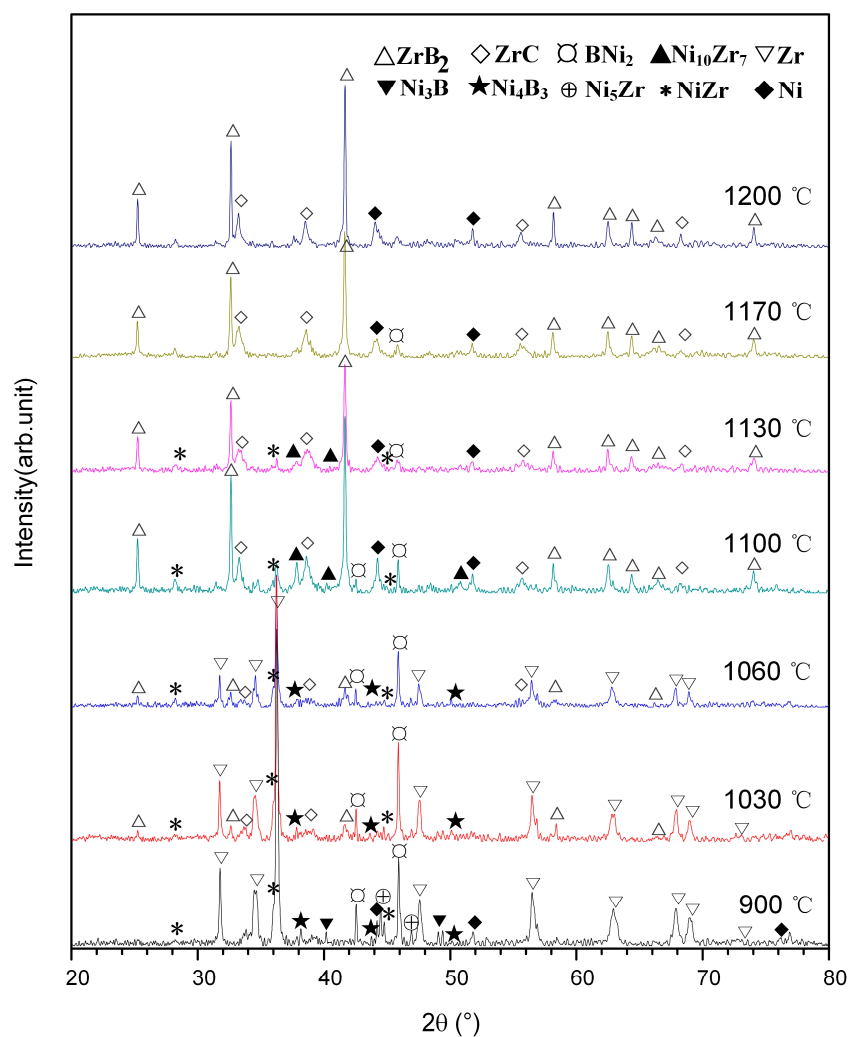


Figure 5. XRD patterns for the DSC products of 30 wt.% Ni-Zr-B₄C mixtures quenched at different temperatures.

In order to better illustrate the above viewpoints, microstructure analysis of DSC quenching products in the 30 wt.% Ni-Zr-B₄C mixture at different temperatures was carried out. The SEM images are shown in Figure 6. It can be seen from Figure 6a that, at room temperature, the raw material mixed powder presented a loose and uniform microstructure. When the temperature was 900 °C, the Ni powder no longer presented a flower shape, but it became denser and bound more closely with the surrounding Zr powder and B₄C powder, as shown in Figure 6b. Some Ni_xB_y compounds formed around it by energy spectrum analysis. When the temperature rose to 1060 °C, the formation of a liquid phase was observed (see Figure 6c). Combining the EDS-point scanning spectrum (see Figure 6g) with the SEM image, point 1 was rich in Ni and B and thus mainly contained the Ni-B liquid phase. When the temperature rose to 1100 °C, the EDS-point scanning spectrum (see Figure 6h) of point 2 in Figure 6d contained Zr, Ni, B and C and, thus, possibly mainly contained the Ni-Zr-B-C liquid phases. When the temperature was further increased to 1170 °C, a large amount of liquid phase was formed, and a small number of ceramic particles were precipitated out of the liquid phase (see Figure 6e). When the temperature was increased to 1200 °C, a large number of ceramic particles formed in the product, as shown in Figure 6f. These results indicate that the microstructure evolution of DSC-quenched products is consistent with the previously inferred reaction mechanism analysis.

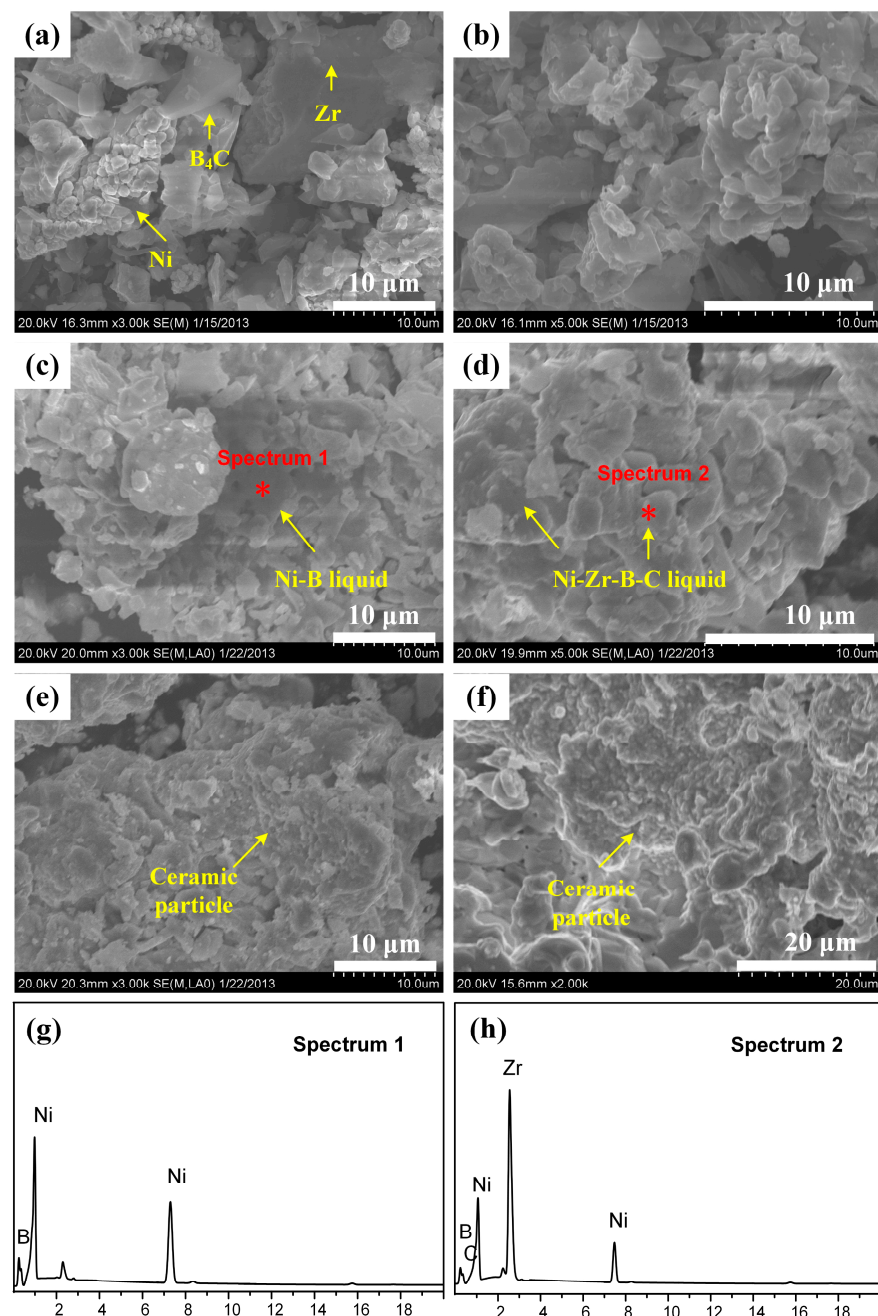


Figure 6. SEM micrographs for the DSC products of 30 wt.% Ni-Zr-B₄C mixtures at (a) room temperature, quenched at (b) 900 °C; (c) 1060 °C; (d) 1100 °C; (e) 1170 °C; (f) 1200 °C; (g,h) the energy-dispersive spectrometry (EDS) spectra of (c,d).

4. Conclusions

Based on DSC and XRD analysis of Zr-B₄C, Ni-B₄C, Ni-Zr and 30 wt.% Ni-Zr-B₄C mixtures, the reaction mechanism in 30 wt.% Ni-Zr-B₄C mixture under DSC conditions is proposed as follows: (i) Firstly, some intermetallic Ni_xB_y (mainly Ni₂B and Ni₄B₃) and Ni_xZr_y (mainly NiZr and Ni₅Zr) formed via solid-state diffusion reactions of Ni, B₄C and Zr at about 851 °C. (ii) Then, Ni₂B and Ni₄B₃ formed a Ni-B eutectic liquid at about 1025 °C, and the free C atoms dissolved into the Ni-B liquid to form a Ni-B-C ternary liquid. When the mixture was heated to about 1088 °C, part of the Zr powder directly reacted with B₄C through a solid-state diffusion reaction, and part of the Zr powder dissolved into the surrounding Ni-B-C ternary liquid to form Ni-Zr-B-C quaternary liquid. (iii) Finally, when

the concentration of [Zr], [B] and [C] in the liquid attained a certain value, ZrB₂ and ZrC formed and precipitated out of the saturated liquid.

Author Contributions: All authors contributed to the study design, data analysis and discussion, as well as to the writing and editing of the manuscript. Study conception and design: J.X., B.Z.; experimental work: J.X., P.M.; data analysis: J.X.; manuscript writing and editing: J.X., P.M. All authors have read and agreed to the published version of the manuscript.

Funding: This research was funded by the National Natural Science Foundation of China (Grant No. 11904126) and the Scientific Research Fund of Jilin Provincial Education Department, China (Grant No. JJKH20200250KJ).

Institutional Review Board Statement: Not applicable.

Informed Consent Statement: Not applicable.

Data Availability Statement: Not applicable.

Conflicts of Interest: The authors declare no conflict of interest.

References

1. Hu, Q.D.; Luo, P.; Zhang, M.X.; Song, M.S.; Li, J.G. Combustion and formation behavior of hybrid ZrB₂ and ZrC particles in Al-Zr-B₄C system during self-propagation high temperature synthesis. *Int. J. Refract. Met. Hard Mater.* **2012**, *31*, 89–95. [[CrossRef](#)]
2. Zhang, M.X.; Huo, Y.Q.; Hu, Q.D.; Zhang, P.; Zou, B.L. Reaction behavior and formation mechanism of ZrC and ZrB₂ in the Cu-Zr-B₄C system. *Int. J. Refract. Met. Hard Mater.* **2014**, *43*, 102–108. [[CrossRef](#)]
3. Zhang, M.X.; Huo, Y.Q.; Huang, M.; Fang, Y.H.; Wang, G.P. The effect of B₄C particle size on the reaction process and product in the Cu-Zr-B₄C system. *J. Asian Ceram. Soc.* **2015**, *3*, 38–43. [[CrossRef](#)]
4. Zhang, M.X.; Zou, B.L.; Xu, J.Y.; Cai, X.L.; Wang, Y.; Huang, M.; Fang, Y.H.; Huo, Y.Q.; Cao, X.Q. Reaction behavior, microstructure and application in coating of in situ ZrC-ZrB₂ ceramic composites powders from a Co-Zr-B₄C system. *Mater. Des.* **2015**, *81*, 65–72. [[CrossRef](#)]
5. Zhang, M.X.; Huo, Y.Q.; Huang, M.; Fang, Y.H.; Zou, B.L. In situ synthesis and formation mechanism of ZrC and ZrB₂ by combustion synthesis from the Co-Zr-B₄C system. *J. Asian Ceram. Soc.* **2015**, *3*, 271–278. [[CrossRef](#)]
6. Hu, Q.D.; Zhao, X.R.; Sun, S.; Zheng, H.; Cao, S.; Li, J.G.; Zhang, M.X. Kinetic role of Cu content in reaction process, behavior and their relationship among Cu-Zr-C system. *J. Mater. Sci. Technol.* **2019**, *35*, 2375–2382. [[CrossRef](#)]
7. Yang, Y.F.; Wang, H.Y.; Zhao, R.Y.; Liang, Y.H.; Jiang, Q.C. Effect of Ni content on the reaction behaviors of self-propagating high-temperature synthesis in the Ni-Ti-B₄C system. *Int. J. Refract. Met. Hard Mater.* **2008**, *26*, 77–83. [[CrossRef](#)]
8. Liang, Y.H.; Wang, H.Y.; Yang, Y.F.; Du, Y.L.; Jiang, Q.C. Reaction path of the synthesis of TiC-TiB₂ in Cu-Ti-B₄C system. *Int. J. Refract. Met. Hard Mater.* **2008**, *26*, 383–388. [[CrossRef](#)]
9. Zhang, Z.Q.; Shen, P.; Jiang, Q.C. Differential thermal analysis (DTA) on the reaction mechanism in Fe-Ti-B₄C system. *J. Alloys Compd.* **2008**, *463*, 498–502. [[CrossRef](#)]
10. Trung, T.B.; Zuhailawati, H.; Ahmad, Z.A.; Ishihara, K.N. Grain growth, phase evolution and properties of NbC carbide-doped WC-10AlSi304 hard metals produced by pseudo hot isostatic pressing. *J. Alloys Compd.* **2013**, *552*, 20–25. [[CrossRef](#)]
11. Balbo, A.; Sciti, D. Spark plasma sintering and hot pressing of ZrB₂-MoSi₂ ultra-high temperature ceramics. *Mater. Sci. Eng. A* **2008**, *475*, 108–112. [[CrossRef](#)]
12. Mashhadi, M.; Taheri-Nassaj, E.; Mashhadi, M.; Sglavo, V.M. Pressureless sintering of B₄C-TiB₂ composites with Al additions. *Ceram. Int.* **2011**, *37*, 3229–3235. [[CrossRef](#)]
13. Yang, Y.F.; Wang, H.Y.; Liang, Y.H.; Zhao, R.Y.; Jiang, Q.C. Fabrication of steel matrix composites locally reinforced with different ratios of TiC/TiB₂ particulates using SHS reactions of Ni-Ti-B₄C and Ni-Ti-B₄C-C systems during casting. *Mater. Sci. Eng. A* **2007**, *445–446*, 398–404. [[CrossRef](#)]
14. Zhu, G.L.; Wang, W.; Wang, R.; Zhao, C.B.; Pan, W.T.; Huang, H.J.; Du, D.F.; Wang, D.H.; Shu, D.; Dong, A.P.; et al. Formation mechanism of spherical TiC in Ni-Ti-C system during combustion synthesis. *Materials* **2017**, *10*, 1007–1014. [[CrossRef](#)] [[PubMed](#)]
15. Jin, S.B.; Su, H.K.; Sha, G. Atom Probe tomography analysis of TiC_x powders synthesized by SHS in Al/Fe/Cu-Ti-C systems. *Materials* **2019**, *12*, 4095–4105. [[CrossRef](#)]
16. Levashov, E.A.; Mukasyan, A.S.; Rogachev, A.S.; Shtansky, D.V. Self-propagating high-temperature synthesis of advanced materials and coatings. *Int. Mater. Rev.* **2017**, *62*, 203–239. [[CrossRef](#)]
17. Zou, B.L.; Xu, J.Y.; Wang, Y.; Zhao, S.M.; Fan, X.Z.; Hui, Y.; Zhou, X.; Huang, W.Z.; Cai, X.L.; Tao, S.Y.; et al. Self-propagating high-temperature synthesis of TiC-TiB₂-based Co cermets from a Co-Ti-B₄C system and fabrication of coatings using the cermet powders. *Chem. Eng. J.* **2013**, *233*, 138–148. [[CrossRef](#)]
18. Liang, Y.H.; Han, Z.W.; Zhang, Z.H.; Li, X.J.; Ren, L.Q. Effect of Cu content in Cu-Ti-B₄C system on fabricating TiC/TiB₂ particulates locally reinforced steel matrix composites. *Mater. Des.* **2012**, *40*, 64–69. [[CrossRef](#)]

19. Dunmead, S.D.; Readey, D.W.; Semler, C.E.; Hol, J.B. Kinetics of combustion synthesis in the Ti-C and Ti-C-Ni systems. *J. Am. Ceram. Soc.* **1989**, *72*, 2318–2324. [[CrossRef](#)]
20. Lasalvia, J.C.; Kim, D.K.; Lipsett, R.A.; Meyers, M.A. Combustion synthesis in the Ti-C-Ni-Mo system: Part I. Micromechanisms. *Metall. Mater. Trans. A* **1995**, *26*, 3001–3009. [[CrossRef](#)]
21. Xu, J.Y.; Zou, B.L.; Zhao, S.M.; Hui, Y.; Huang, W.Z.; Zhou, X.; Wang, Y.; Cai, X.L.; Cao, X.Q. Fabrication and properties of ZrC-ZrB₂/Ni cermet coatings on a magnesium alloy by atmospheric plasma spraying of SHS powders. *Ceram. Int.* **2014**, *40*, 15537–15544. [[CrossRef](#)]
22. Massalski, T.B.; Okamoto, H.; Subramanian, P.R. *Binary Alloy Phase Diagrams*, 2nd ed.; ASM International: Metals Park, OH, USA, 1990.
23. Hayes, E.T.; Roberson, A.H.; Paasche, O.G. The Zirconium-Nickel phase diagram. *Trans. ASM* **1953**, *45*, 893–900.